Supporting Information for "Joint inversion of co-seismic and early post-seismic slip to optimize the information content in geodetic data: Application to the 2009 M_w6.3 L'Aquila earthquake, Central Italy"

Théa Ragon[1], Anthony Sladen[1], Quentin Bletery[1], Mathilde Vergnolle[1], Olivier Cavalié[1], Antonio Avallone[2], Julien Balestra[1], Bertrand Delouis[1]

[1]Université Côte d'Azur, CNRS, Observatoire de la Côte d'Azur, IRD, Géoazur, Valbonne, France
[2]Istituto Nazionale di Geofisica e Vulcanologia, Rome, Italy

Contents

Text S1. Description of the observations

The strictly co-seismic dataset contains static offsets analyzed from the 31 1 Hz-sampled and the two 10 Hz-sampled high rate GPS stations located in the earthquake area. Strictly co-seismic offsets have been calculated from the difference on the 3 components between mean position before the event ([t_0-5 s : t_0]) and after the event ([t_0+25 s : t_0+30 s]) [*Avallone et al.*, 2011]. Data errors are used to build a diagonal covariance matrix $\mathbf{C}_\mathrm{d}^\mathrm{gps}$ describing observational uncertainties.

The 6 days of co and early post-seismic dataset contains 40 static GPS offsets and 2 InSAR frames. We consider the continuous GPS sites included in *Cheloni et al.* [2010] and 2 survey style GPS sites. Offsets have been calculated from the difference on the 3 components between mean position before the event and 6 days after the event. Mean values and relative uncertainties have been calculated for a time interval of 7 days before t_0 and on the period between 5 and 7 days after t_0. This approach mirrors the high rate GPS analysis [*Avallone et al.*, 2011] and allows to calculate reliable uncertainties on the 3 days period around the 6th day after earthquake. Uncertainties are added to the observational errors matrix $\mathbf{C}_\mathrm{d}^\mathrm{gps}$. Additionally, two post-seismic COSMO-SkyMed and ENVISAT images have been acquired the October 12th 2009, 6 days after the mainshock. Two differential interferograms have thus been generated, each containing co-seismic displacement and 6 days of post-seismic signal: an ascending COSMO-SkyMed frame and a descending Envisat frame (Tab. S1). The interferograms have been processed using the JPL/Caltech ROI_PAC software [*Rosen et al.*, 2004]. To improve computational efficiency, we resample InSAR observations based on model resolution [*Lohman and Simons*, 2005] with windows ranging from 12 km to 1 km. We account for measurement uncertainties by building a data covariance matrix. To do so, we mask the area of coseismic displacement and estimate empirical covariograms as a function of distance between data points (Figure S2). Then, the InSAR covariance matrix $\mathbf{C}_\mathrm{d}^\mathrm{insar}$ is calculated from the best fitting exponential function to empirical covariograms [*Jolivet et al.*, 2012].

Corresponding author: Théa Ragon, ragon@geoazur.unice.fr

Supplementary Tables

Satellite (orbit pass)	Interferogram pair	Mean incidence angle
COSMO-SkyMed (ascending)	04/04/2009 - 12/04/2009	35.9
Envisat (descending)	24/04/2008 - 12/04/2009	23

Table S1. Interferometric pairs used in this study.

	CTW approach, with C_p COpref and POSTpref	**CTW approach, no C_p** sCO and sPOST	**Strictly Coseismic, no C_p** COgps	**Co+post-seismic no C_p** CO+POST
GPS, co-seismic	1.19	1.14	1.13	1.43
GPS, 6 days offset	0.899	0.697	1.22	0.826
COSMO-SkyMed asc.	4.11	3.98	8.82	3.96
Envisat dsc.	1.76	2.02	10.1	1.88

Table S2. Residuals between observations and predictions (RMS in centimetre) for slip models inferred within the CTW approach, accounting or not for $\mathbf{C}_\mathrm{p}$, and for slip models inferred independently: strictly co-seismic slip model and co and post-seismic slip model, without accounting for $\mathbf{C}_\mathrm{p}$.

Supplementary Figures

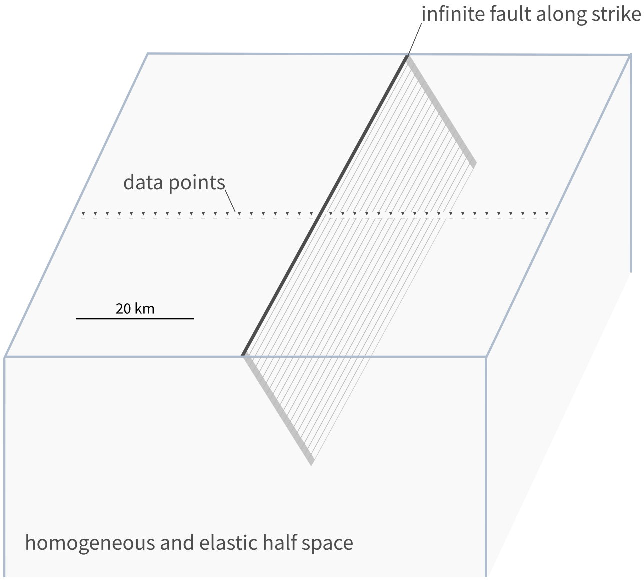

Figure S1. Schematic view of the 2D simplified toy model we use to explore the impact of the CTW approach on the inferred models. The assumed fault extends infinitely along strike, but is discretized into 20 subfaults of 1 km width. The synthetic data are distributed along a profile line perpendicular to the fault strike, centred on the fault at the surface. There are 100 data points that are spaced every kilometer. The medium is a homogeneous and elastic half space.

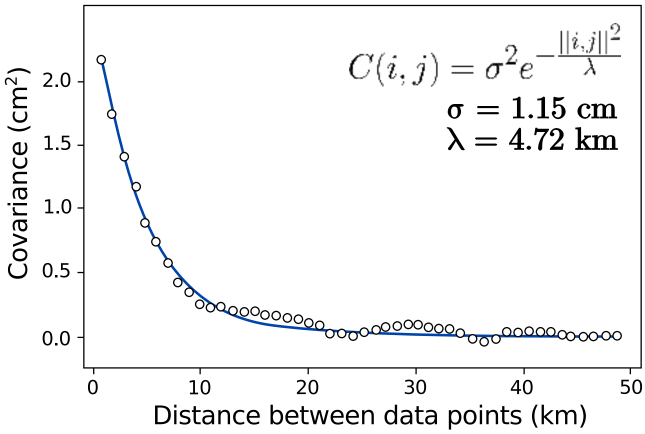

Figure S2. Empirical covariance functions for the Envisat descending interferogram. One dimensional empirical covariance functions and associated best fit exponential functions for the displacements derived from InSAR data. For each interferogram, we compute the empirical covariance as a function of the inter-pixel distance and then fit an exponential function (Jolivet et al. 2012). The exponential function is used to build the data covariance matrix.

Figure S3. The set of samples inferred from an inversion is divided into 25 families. The first family gathers samples whose parameters deviate of less than 50 cm from the median model parameters (for the co-seismic slip). In detail, a model is added to the first family if the selected model and the median model are parameter-wise equal within a tolerance of 50 cm for the co-seismic slip, and a tolerance of 25 cm for the post-seismic slip. Other families are built iteratively around a randomly selected model that has not fitted within antecedent families, except for the last family which gathers orphan samples. (continued)

Figure S3. (Previous page.) In (a), the median model of each family is shown for the co-seismic slip model inferred accounting for $\mathbf{C}_\mathrm{p}$ with the CTW approach. In (b), one sample is selected randomly in each of the 25 subsets. Figures 3a-d and 5a-b illustrate the median parameters of the 25 families of (a) for each subfault: for instance, the top right pixels of each subfault in Figure 5a correspond to the parameters of the median model of the first family shown in (a).

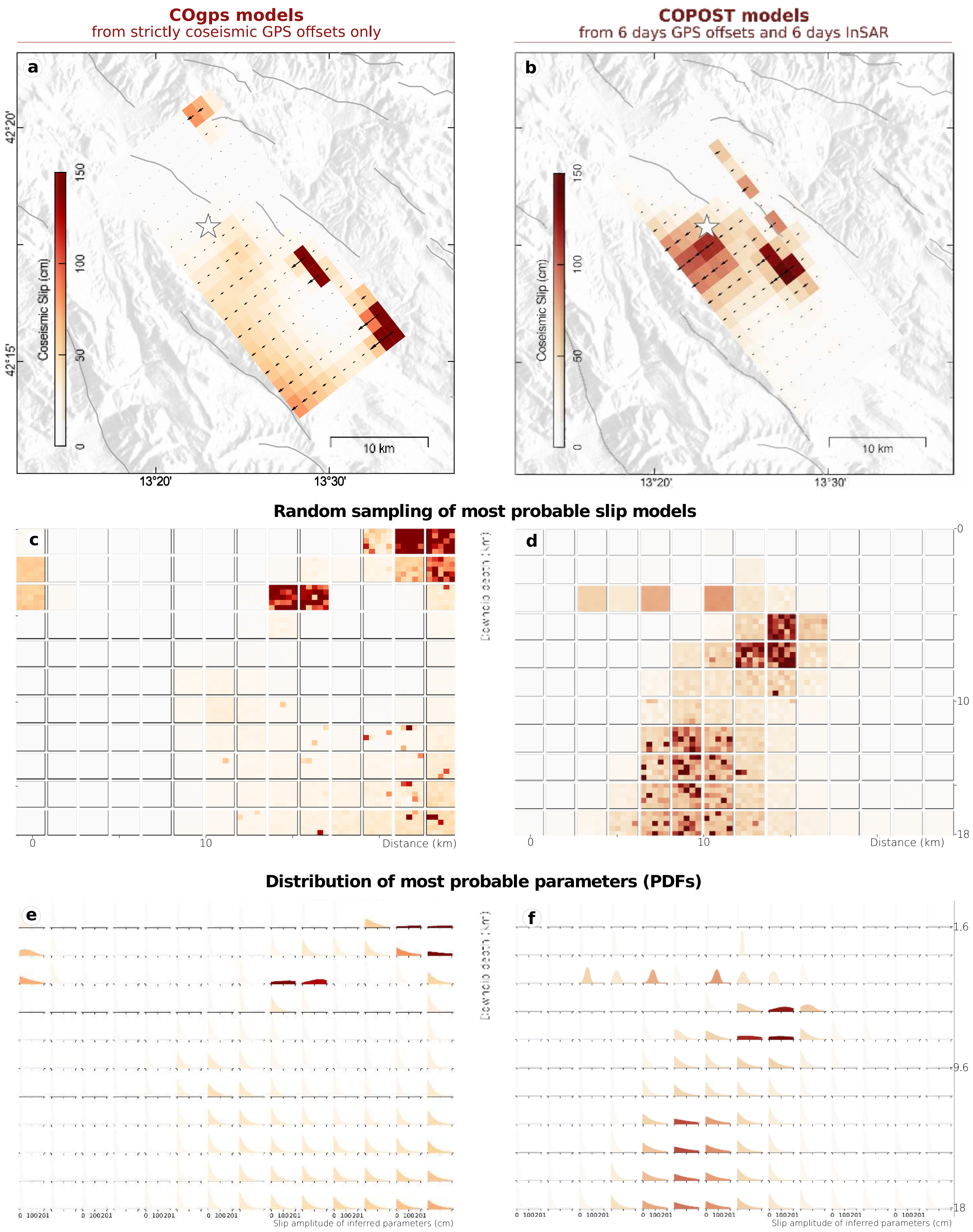

Figure S4. Finite-fault slip models inferred from strictly co-seismic data (model COgps) or data including the co-seismic phase plus some early post-seismic deformation (model COPOST). (a) and (b) show the slip amplitude and rake of the median model, the epicenter being the white star. The color scale is the same for all the figures. (c) and (d) illustrate the slip amplitude of the median models of 25 families of inferred models (more information in the text and Figure S4). This presentation allows a visual estimation of the covariance between probable models at the scale of subfaults. (e) and (f) represent the posterior probability density functions of the 300000 samples for each model parameter, and thus the amount of samples that have inferred slip values for each subfault. The PDFs are colored from the median model, the color-scale being the same as in (a) and (b) respectively.

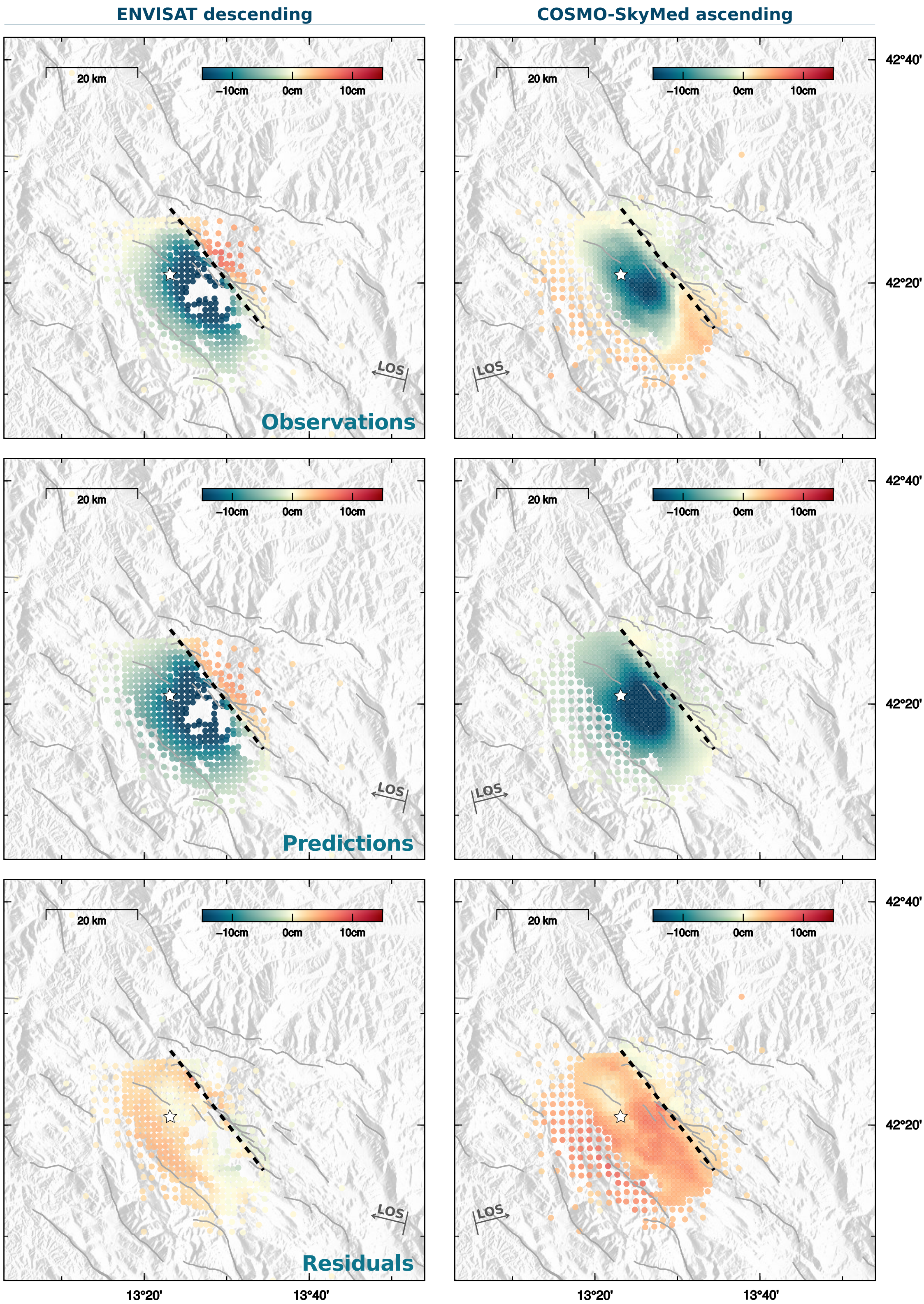

Figure S5. Fit to the InSAR dataset for the median COPOST model. Observations, predictions inferred from the average model and residuals are shown for ENVISAT descending and COSMO-SkyMed ascending interferograms, respectively to the left and to the right. The assumed fault trace is shown with a dotted black line. The epicenter is the white star. Seismogenic faults are shown in light gray.

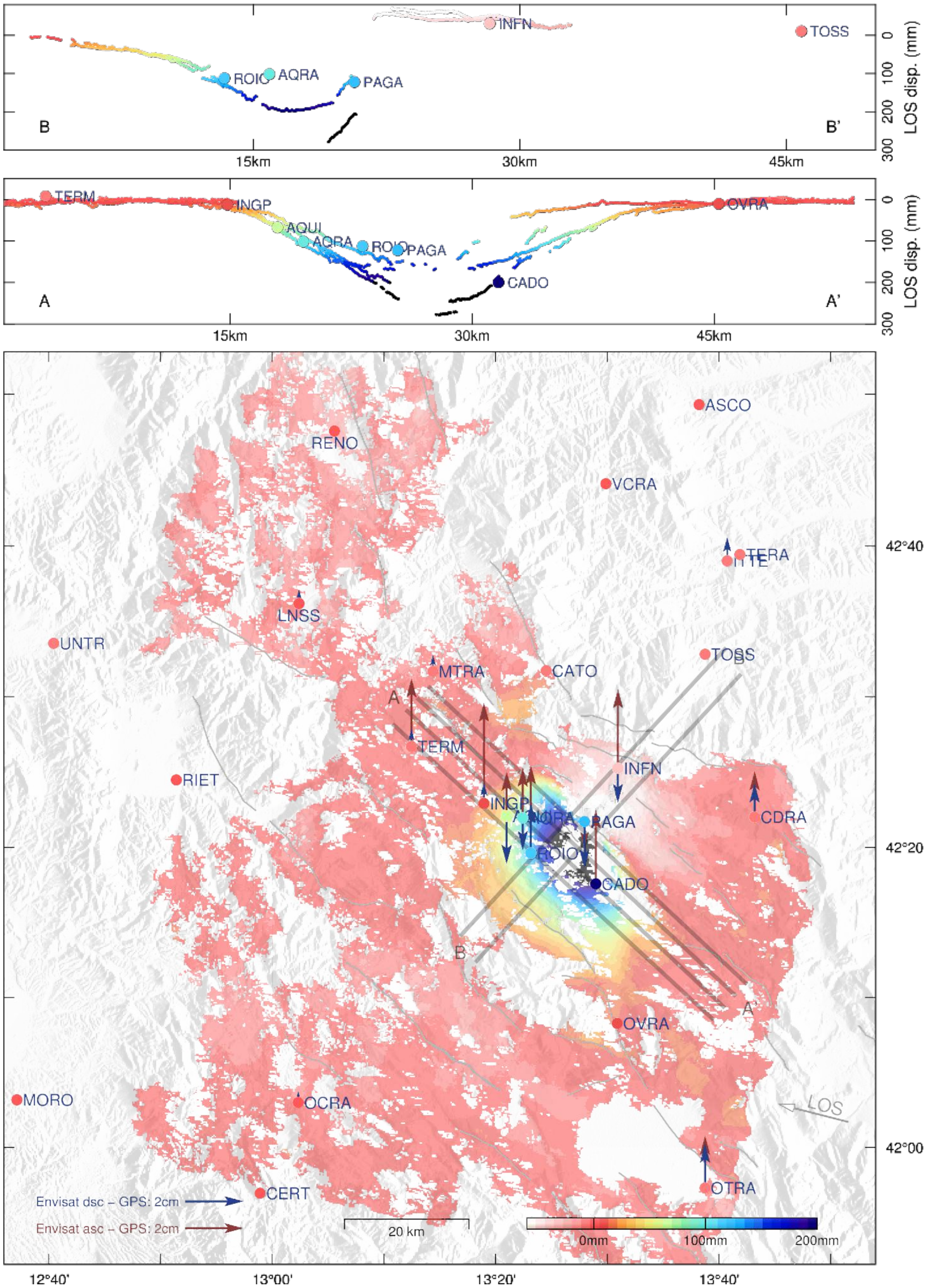

Figure S6. Comparison between co+post GPS and InSAR datasets. The ENVISAT interferogram is shown in background. GPS offsets between mainshock and 6 days after in the Line of Sight (LOS) direction are shown in colored dots in the same colorscale. The offset between surface displacement in the LOS direction of ENVISAT interferogram and GPS is shown with dark blue arrows. Four NW-SE profiles (A - A') and two SW-NE profiles (B - B') represent the LOS displacement of InSAR points along these profiles and of adjacent GPS stations.

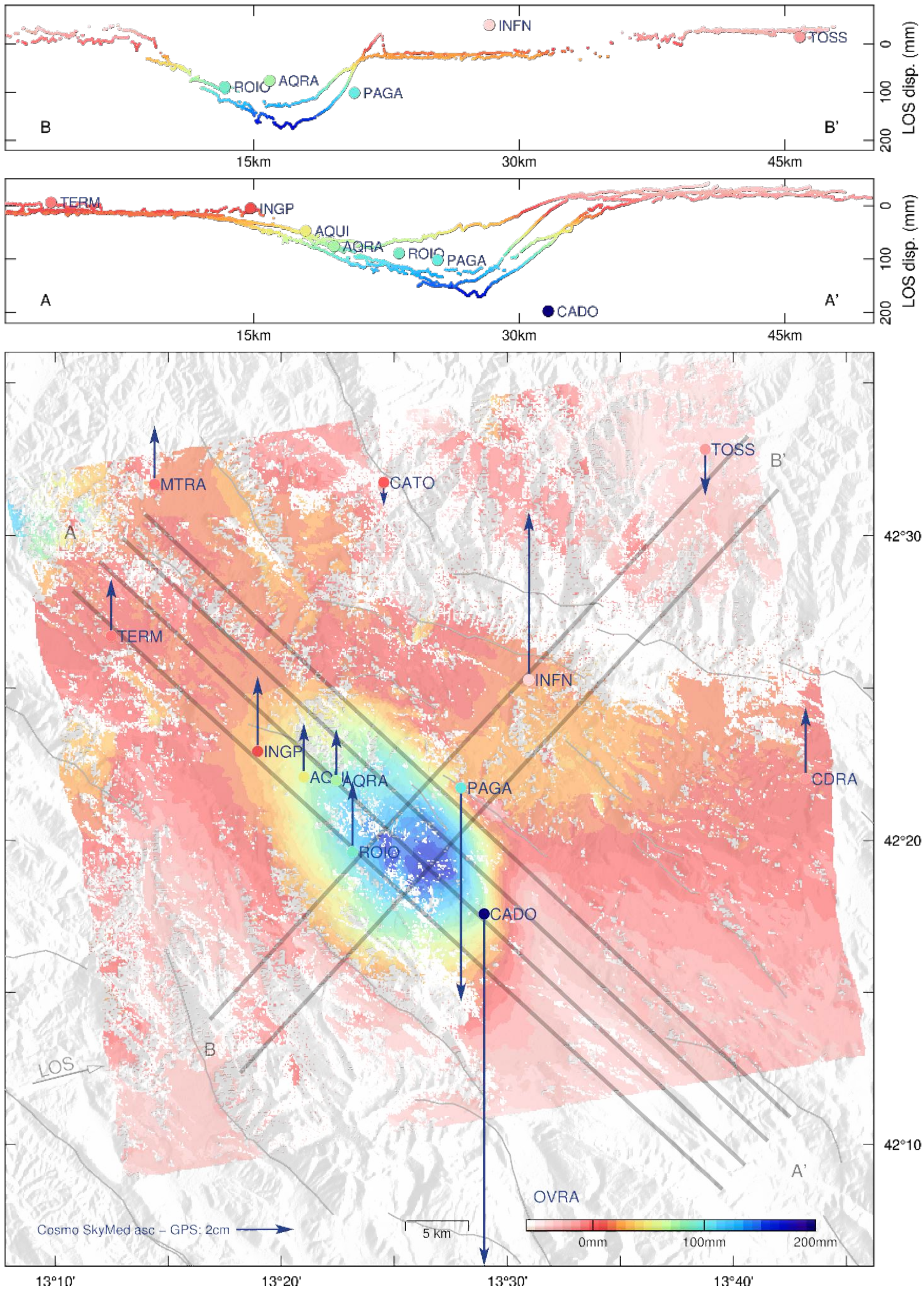

Figure S7. Comparison between co+post GPS and InSAR datasets. The COSMO-SkyMed interferogram is shown in background. GPS offsets between mainshock and 6 days after in the Line of Sight (LOS) direction are shown in colored dots in the same colorscale. The offset between surface displacement in the LOS direction of COSMO-SkyMed interferogram and GPS is shown with dark blue arrows. Four NW-SE profiles (A - A') and two SW-NE profiles (B - B') represent the LOS displacement of InSAR points along these profiles and of adjacent GPS stations.

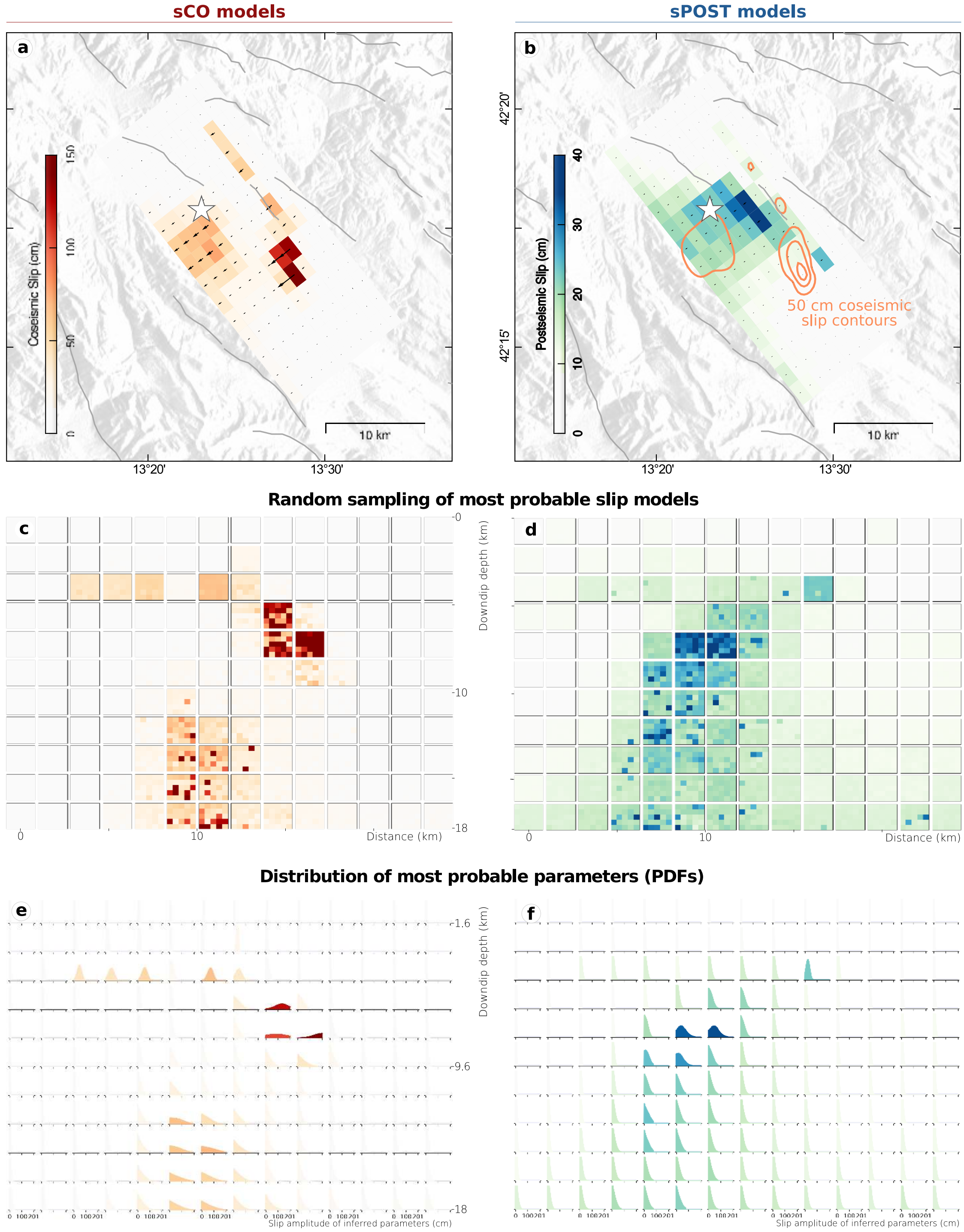

88 **Figure S8.** Strictly co-seismic (model sCO) and early postseismic (model sPOST) finite fault slip models, inferred with the CTW approach and without accounting for epistemic uncertainties. (a) and (b) show the slip amplitude and rake of the median model, the epicenter being the white star. In (b), orange lines also show the 50 cm co-seismic slip contours. The color scale is the same for all the figures. (c) and (d) illustrate the slip amplitude of the median models of 25 families of inferred models. (e) and (f) represent the posterior probability density functions of the 300000 samples for each model parameter. The PDFs are colored from the median model, the color-scale being the same as in (a) and (b) respectively.

Figure S9. Animated slip distribution of the model sCO. We divide our 300000 most probable models into 25 families of models. We then select randomly a sample of each family: the parameters of each sample are depicted by colored pixels in corresponding subfaults for the first step of the animation. Another random set of 25 samples is selected and represented in the second step of the animation, and so forth.
To launch the animation, click on the image. The animation will display in Acrobat Reader preferably. If not displayed, you can find the same animation at the following address: https://ragonthea.wordpress.com/research/fault_geom/

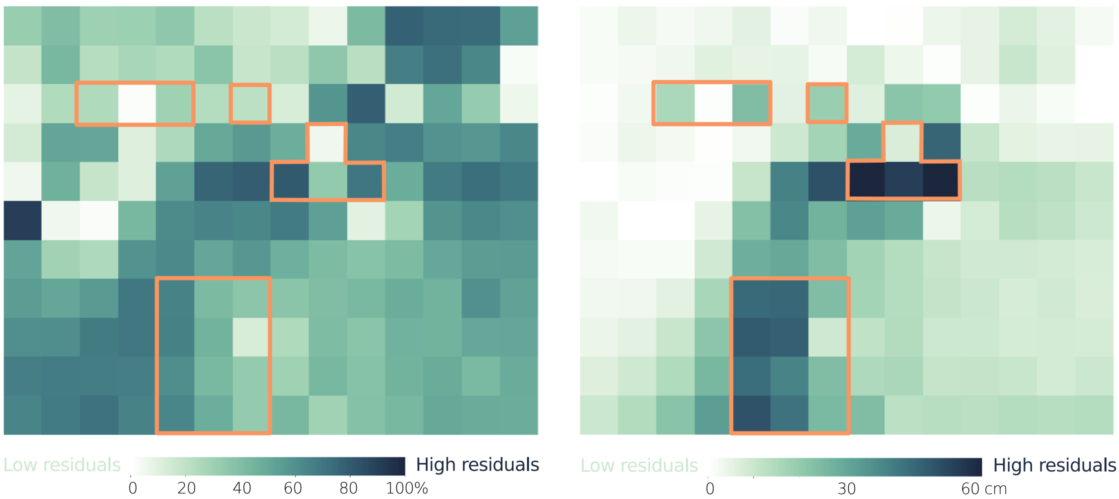

Figure S10. Comparison between the median models sCO and COPOST. Left, the residuals in percentage of slip amplitude for each subfault are shown. Right, the residuals in cm are shown. The orange lines delimit the area in which slip amplitude is greater than 60 cm.

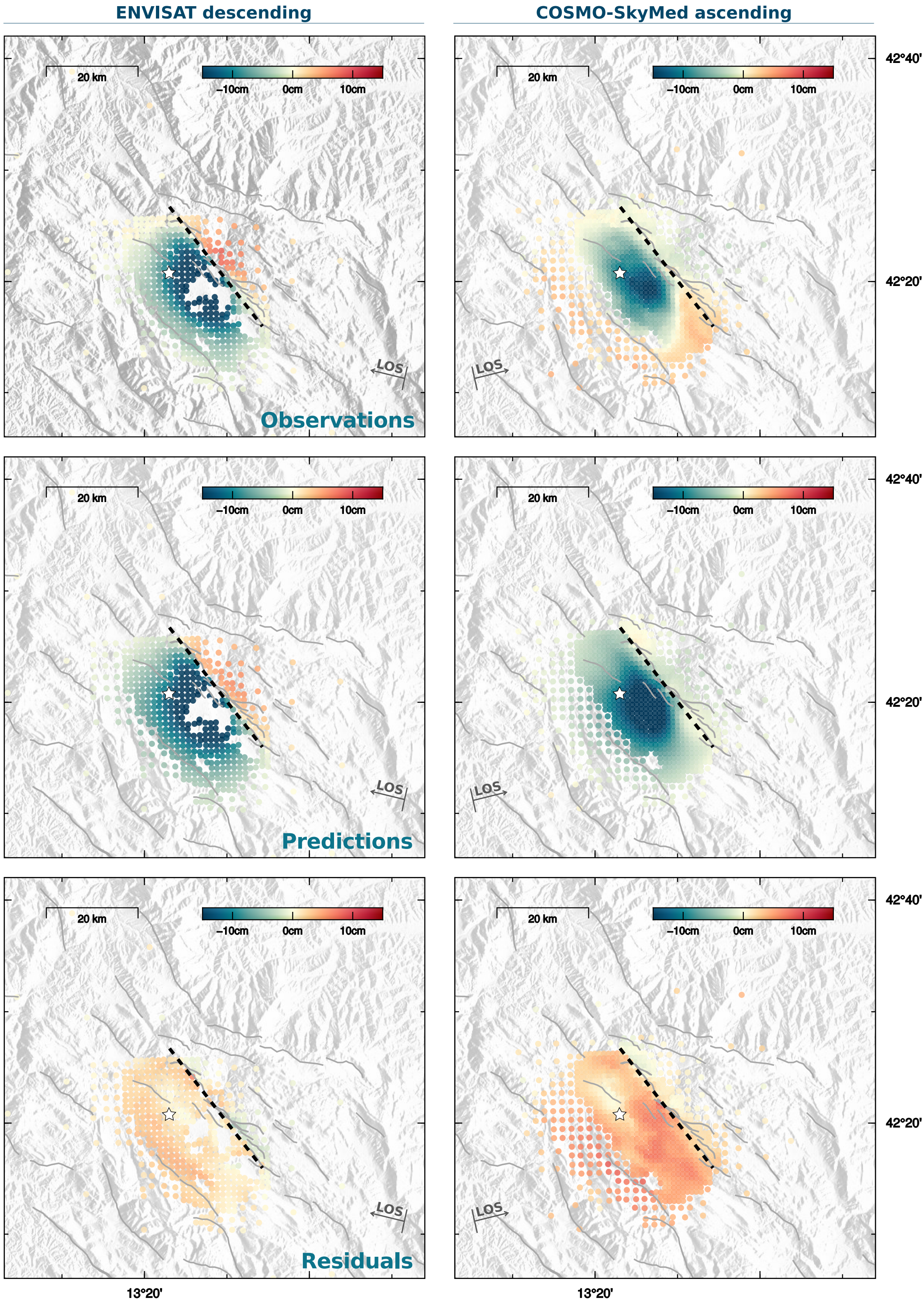

Figure S11. Fit to the InSAR dataset for the median models sCO and sPOST. Observations, predictions inferred from the average model and residuals are shown for ENVISAT descending and COSMO-SkyMed ascending interferograms, respectively to the left and to the right. The assumed fault trace is shown with a dotted black line. The epicenter is the white star. Seismogenic faults are shown in light gray.

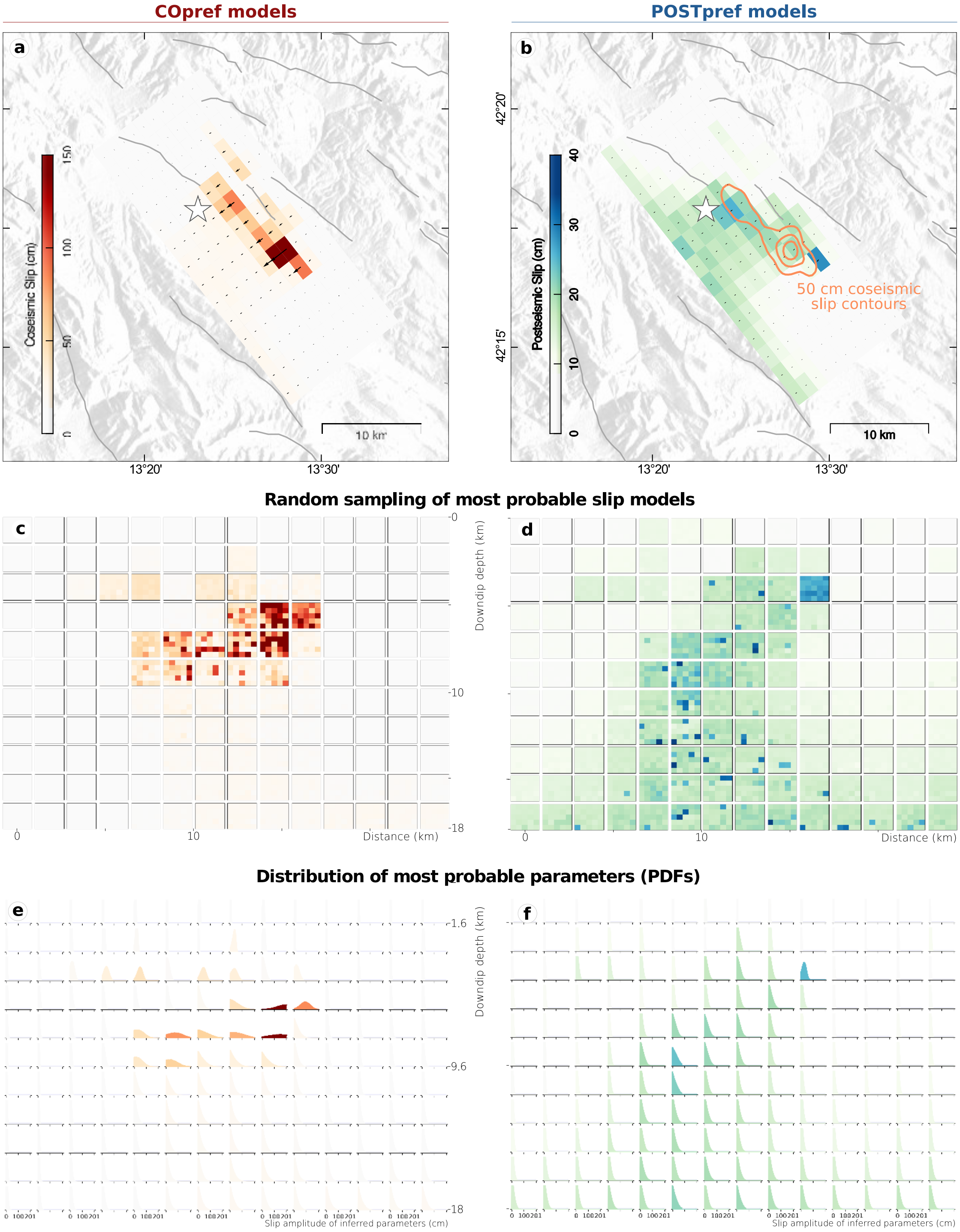

Figure S12. Our preferred models COpref and POSTpref, inferred with the CTW approach and accounting for epistemic uncertainties. (a) and (b) show the slip amplitude and rake of the average model, the epicenter being the white star. In (b), orange lines also show the 50 cm co-seismic slip contours. The color scale is the same for figures a,c,e and b,d,f. (c) and (d) illustrate the slip amplitude of the median models of 25 families of inferred models. (e) and (f) represent the posterior probability density functions of the 300000 samples for each parameter, and thus the amount of samples that have inferred slip values for each subfault. The PDFs are colored from the median model, the color-scale being the same as in (a) and (b) respectively.

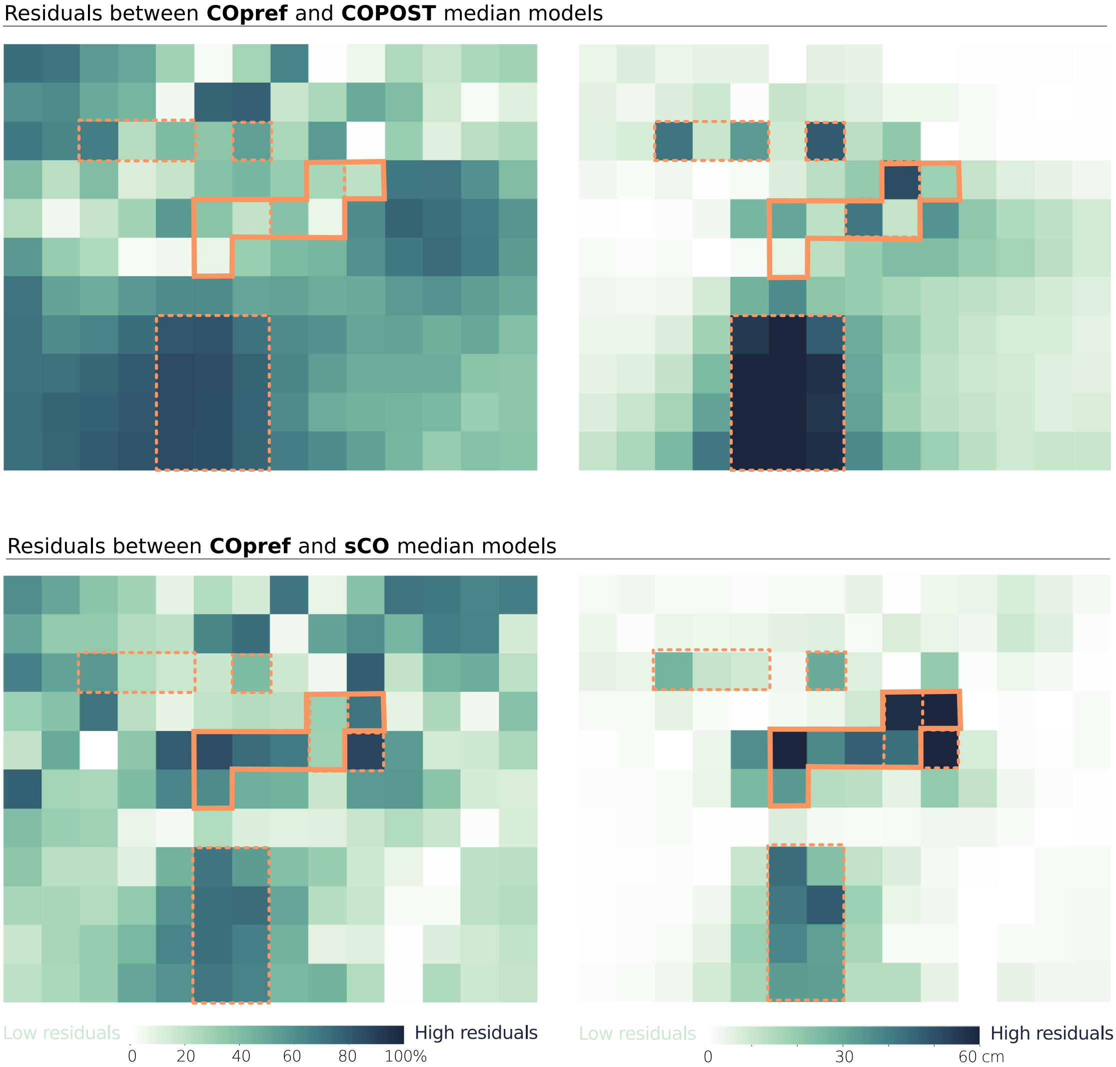

Figure S13. Comparison between our median model COpref and COPOST (top) or sCO (bottom). Left, the residuals in percentage of slip amplitude for each subfault are shown. Right, the residuals in cm are shown. The orange lines delimit the area in which the slip amplitudes of model COpref exceed 50 cm. The dotted orange line delimit these area for model COPOST (top) or model COpref (bottom). The residuals with the COPOST model (top) are largest for the deepest parts of the fault, reaching 90%. The residuals with the sCO model (bottom) exceed 60% for high slip area.

Figure S14. Animated slip distribution of the COpref model. We divide our 300000 most probable models into 25 families of models. We then select randomly a sample of each family: the parameters of each sample are depicted by colored pixels in corresponding subfaults for the first step of the animation. Another random set of 25 samples is selected and represented in the second step of the animation, and so forth.

To launch the animation, click on the image. The animation will display in Acrobat Reader preferably. If not displayed, you can find the same animation at the following address: https://ragonthea.wordpress.com/research/fault_geom/

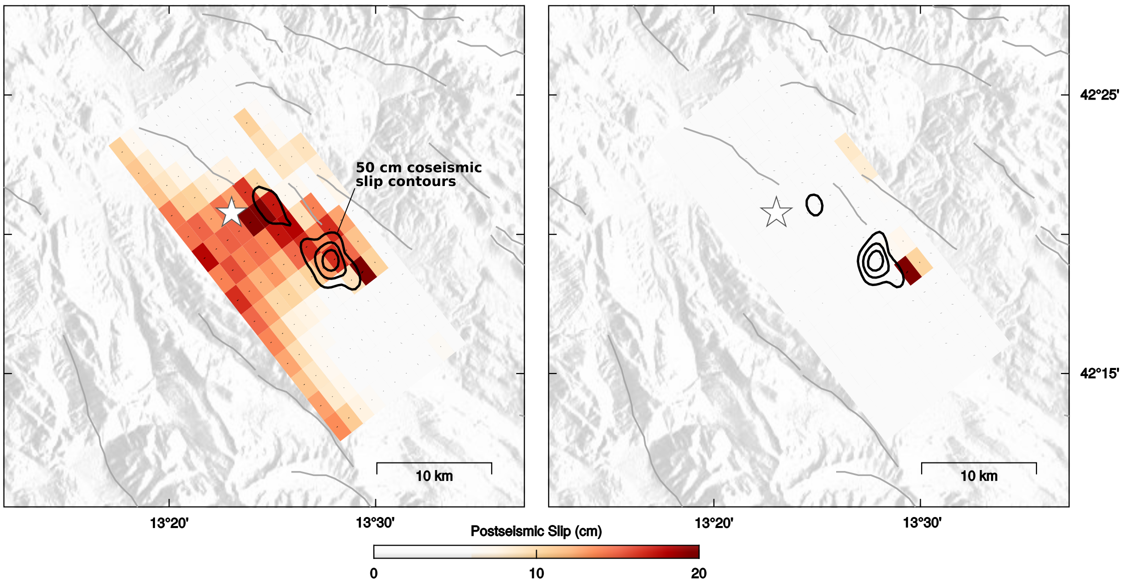

Figure S15. Comparison between two POSTpref models. The coseismic slip is well constrained and do not vary between the median model (left) and the maximum a posteriori (right, mode of the gaussian posterior distributions of inferred samples) model: the 50 cm contours are shown in black lines. In contrast, the posterior uncertainty of the post-seismic slip is large at depth, and median model (left) differs largely from the maximum a posteriori model (right). The most probable post-seismic slip area are the ones imaged by the model to the right, as shared by most inferred samples. The area of large slip as imaged by the median model and with a small posterior uncertainty are also as probable.

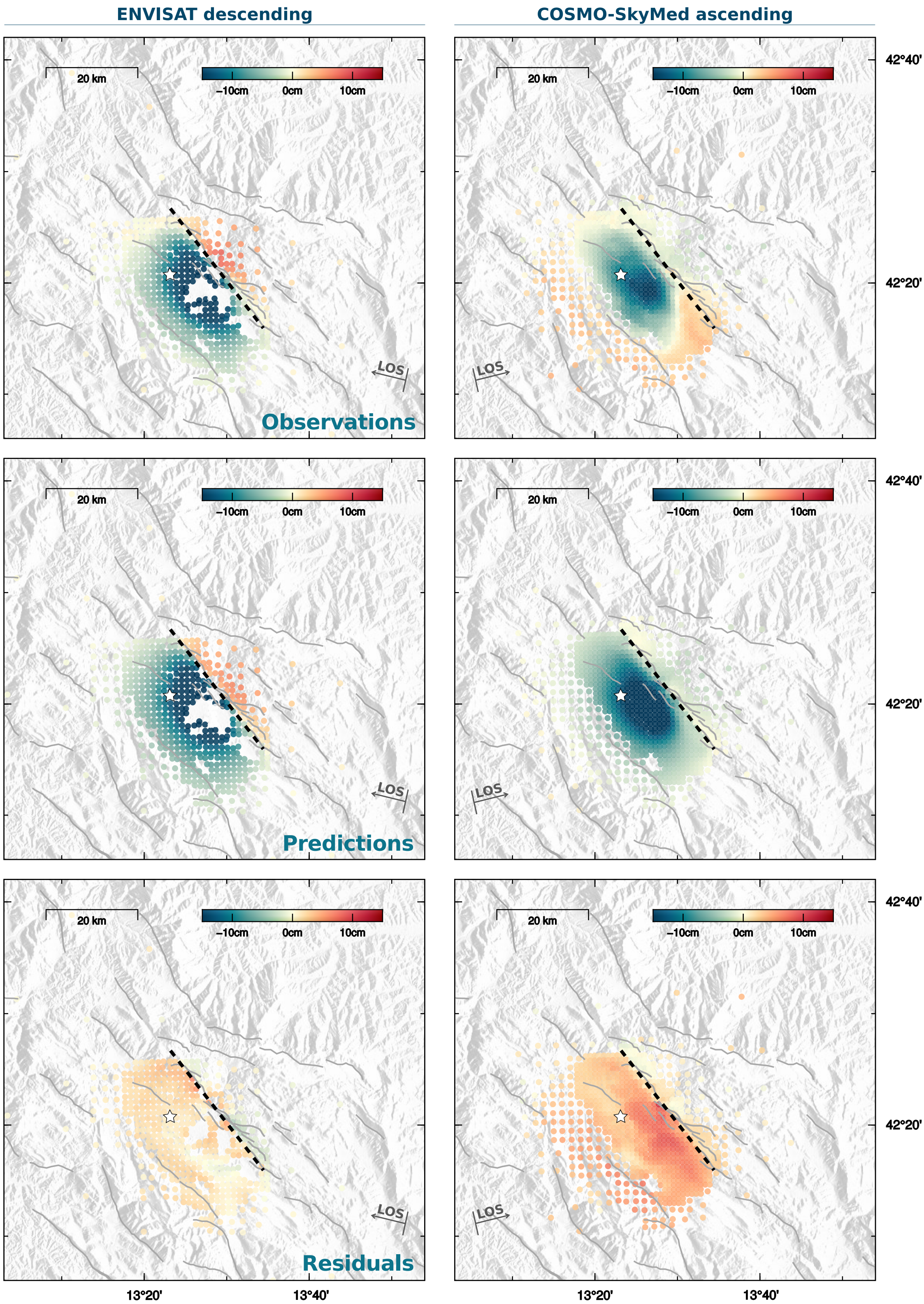

Figure S16. Fit to the InSAR dataset for the median COpref and POSTpref models. Observations, predictions inferred from the average model and residuals are shown for ENVISAT descending and COSMO-SkyMed ascending interferograms, respectively to the left and to the right. The assumed fault trace is shown with a dotted black line. The epicenter is the white star. Seismogenic faults are shown in light gray.

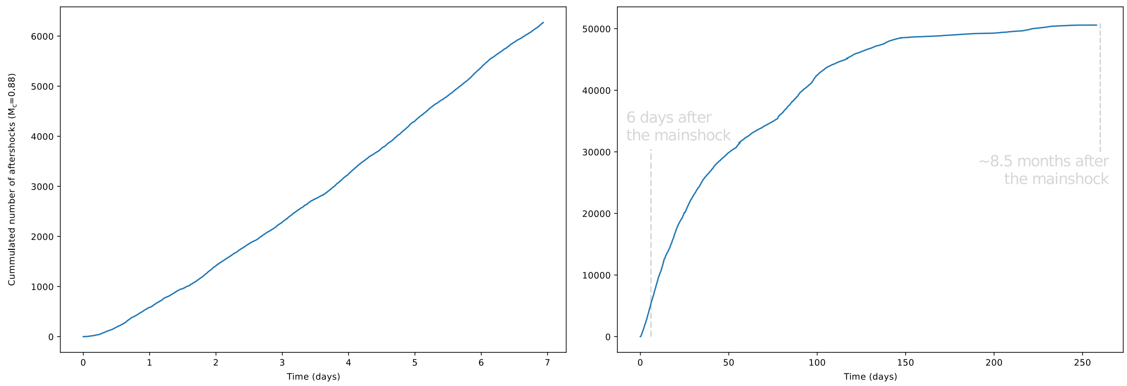

140 **Figure S17.** Cumulative number of events versus time for 6 days after the mainshock (left) or the year
141 2009 (right). The magnitude of completude is of 0.88 [*Valoroso et al.*, 2013]. The increase around 80 days
142 corresponds to the nucleation of several earhquakes of $M_w \approx 4$ [*Chiaraluce et al.*, 2011].